Importance of Ligand Bioactive Conformation in the Discovery of Potent Indole-Diamide Inhibitors of the Hepatitis C Virus NS5B

Steven R. LaPlante,* James R. Gillard, Araz Jakalian, Norman Aubry,
René Coulombe, Christian Brochu, Youla S. Tsantrizos, Martin Poirier,
George Kukolj, and Pierre L. Beaulieu

*Departments of Chemistry and Biological Sciences, Boehringer Ingelheim (Canada) Ltd.,
2100 Cunard St., Laval, Quebec, Canada, H7S2G5*

Received February 24, 2010; E-mail: steven.laplante@boehringer-ingelheim.com

Abstract: Significant advances have led to receptor induced-fit and conformational selection models for describing bimolecular recognition, but a more comprehensive view must evolve to also include ligand shape and conformational changes. Here, we describe an example where a ligand's "structural hinge" influences potency by inducing an "L-shape" bioactive conformation, and due to its solvent exposure in the complex, reasonable conformation-activity-relationships can be qualitatively attributed. From a ligand design perspective, this feature was exploited by successful linker hopping to an alternate "structural hinge" that led to a new and promising chemical series which matched the ligand bioactive conformation and the pocket bioactive space. Using a combination of X-ray crystallography, NMR and modeling with support from binding-site resistance mutant studies and photoaffinity labeling experiments, we were able to derive inhibitor-polymerase complexes for various chemical series.

Introduction

The binding of small ligands to macromolecules involves many events that commonly include the establishment of hydrogen-bonds, van der Waals surface contacts, lipophilic interactions, and ionic attractions.[1] Equally important are some less characterized events that contribute to ligand−receptor interactions. These may include, for example, desolvation effects and conformational changes of the ligand and receptor. However, optimization of ligand binding, one of the primary goals of medicinal chemistry, is often confounded by the reality that each complex entails a unique combination of the above events. Unfortunately, the deconvolution and importance of the individual energetic contributions have often proven to be very difficult or impossible.

In addressing conformational changes, significant advances have led to receptor-induced fit and conformational selection models for describing bimolecular recognition, but a more comprehensive view must evolve to also include ligand shape and conformational changes.[1,2] Binding may be viewed as the collision of two flexible objects, where their transient shapes must have sufficient complementarity to form the encounter complex, that is followed by mutual adaptations to stabilize the interaction. Deciphering the details of the collision and binding events (i.e., adaptations and energetic contributions) remains largely elusive and impractical in drug discovery.

Here, we describe an example where a ligand's "structural hinge" influences potency by inducing an "L-shape" bioactive conformation, and due to its solvent exposure in the complex, reasonable conformation-activity-relationships can be qualitatively attributed. This feature was exploited where successful linker hopping to an alternate "structural hinge" led to a new and promising chemical series which matches the ligand bioactive conformation and the pocket bioactive space. Revealing complexes with HCV polymerase are disclosed. It is also noteworthy that the combination of strategies employed for monitoring ligand structure and dynamics properties, in concert with medicinal chemistry as described here, should have general drug design utility.

There is certainly an urgent need for drugs that specifically target HCV as it is estimated that 1−3% of of the world population are infected. HCV infections may lead to serious and often fatal liver diseases such as cirrhosis and hepatocellular carcinomas. The current treatment option consists of pegylated interferon−ribavirin combinations; however, the treatment has limited efficacy against the major genotype 1 of HCV and can have severe side effects. In industrialized nations, HCV infection has become the major cause for liver transplantation.[3a,b] NS5B

(1) (a) Teague, S. *Nature Rev. Drug Disc.* **2003**, *2*, 527–541. (b) Weikl, T. R.; von Deuster, C. *Proteins: Structure, Function, and Bioinformatics* **2009**, *75*, 104–110. (c) Hammes, G. G.; Chang, Y. C.; Oas, T. G. *Proc. Natl. Acad. Sci. U.S.A.* **2009**, *106*, 13737–13741. (d) Bakan, A.; Bahar, I. *Proc. Natl. Acad. Sci. U.S.A.* **2009**, *106*, 14349–14354. (e) Lakomek, N. A.; Lange, O. F.; Oliver, F.; Walter, K. F.; Korvin, F. A.; Fares, C.; Egger, D.; Lunkenheimer, P.; Meiler, J.; Grubmueller, H.; Becker, S.; de Groot, B. L.; Griesinger, C. *Biochem. Soc. Trans.* **2008**, *36*, 1433–1437. (f) Lange, O. F.; Lakomek, N. A.; Fares, C.; Schroeder, G. F.; Gunnar, G.; Walter, K. F. A.; Becker, S.; Meiler, J.; Grubmueller, H.; Griesinger, C.; de Groot, B. L. *Science* **2008**, *320*, 1471–1475. (g) Kern, D.; Zuiderweg, E. R. *Curr. Opin. Struct. Biol.* **2003**, *13*, 748–757. (h) Mittermaier, A.; Kay, L. E. *Science* **2006**, *312*, 224–228.

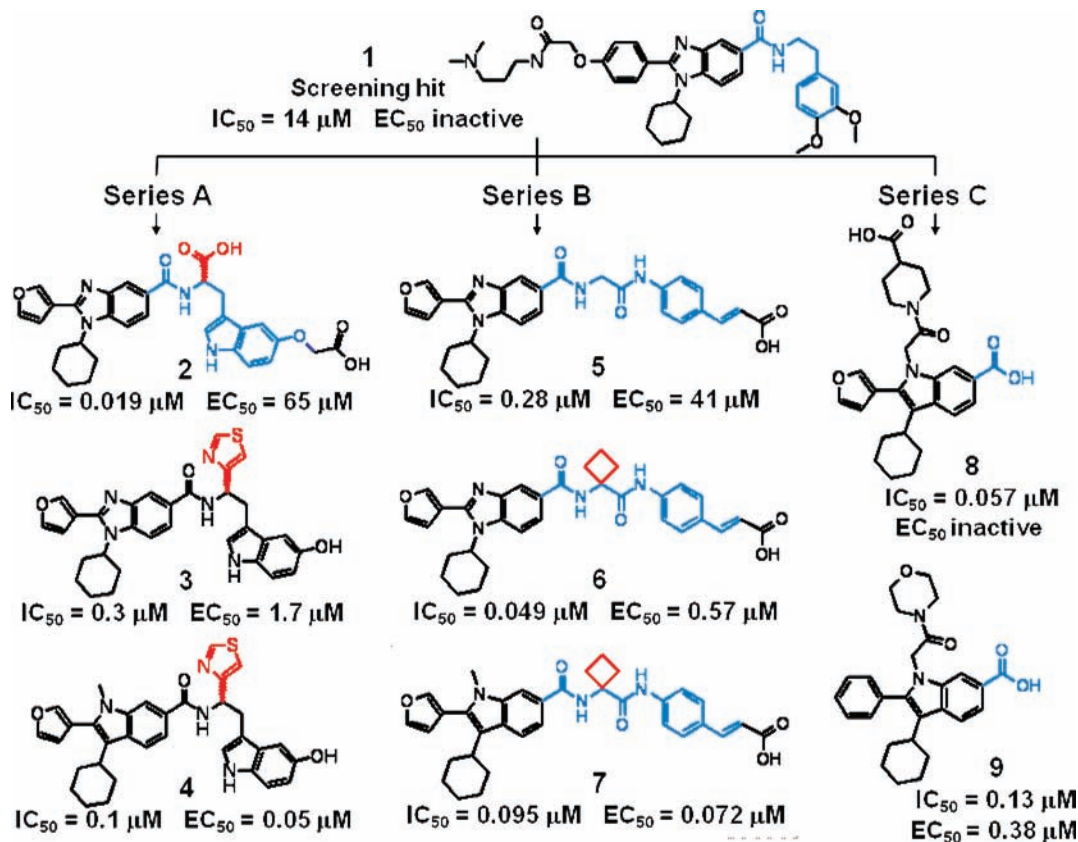(2) Koshland, D. *Adv. Enzymol. Relat. Subj. Biochem.* **1960**, *22*, 45–97.

Figure 1. Compounds derived from three HCV polymerase drug discovery series are shown. The structures are colored as described in the text. Methods for determining activities against HCV NS5B polymerase (genotype 1b) are also described in the Supporting Information and elsewhere.[9g] The activity values are the mean from multiple determinations with the following IC_{50} and EC_{50} standard deviations, respectively: **1**, ± 2.6; **2**, ± 0.006, ± 25; **3**, ± 0.12, ± 0.48; **4**, ± 0.08, ± 0.009; **5**, ± 0.07, ± 20[a]; **6**, ± 0.05, ± 0.2; **7**, ± 0.042[a], ± 0.03; **8**, ± 0.003; **9**, ± 0.07[a], ± 0.12. [a]Standard deviations were overestimated at 50% of the activity values but are typically much less.

RNA-dependent RNA polymerase is already promising to be a valid target for the development of novel anti-HCV therapeutics. Recently, nucleoside analogs and non-nucleoside allosteric inhibitors of the enzyme have demonstrated efficacy in the clinic, particularly in combination with interferon-based regimens.[3c−e] This work discloses novel compounds that are among the most potent reported for allosteric "thumb pocket I" inhibitors of the

hepatitis C virus (HCV) NS5B polymerase, and close analogues of compound **7** (Figure 1) are now reported in patents and in clinical trials.[3f,g]

Results and Discussion

Even though constraining the conformation of inhibitors has been recognized as an important strategy in drug design,[4] relatively few reports have extensively characterized ligand free-state flexibility and conformational changes upon binding to macromolecules.[5] The importance of an inhibitor's shape and

(3) (a) Choo, Q.-L.; Kuo, G.; Weiner, A. J.; Overby, L. R.; Bradley, D. W.; Houghton, M. *Science* **1989**, *244*, 359. (b) Lavanchy, D. *Liver Int.* **2009**, *29*, 74. (c) O'Brien, C.; Godofsky, E.; Rodriguez-Torres, M.; Afdhal, N.; Pappas, S. C.; Pockros, P.; Lawitz, E.; Bzowej, N.; Rustgi, V.; Sulkowski, M.; Sherman, K.; Jacobson, I.; Chao, G.; Knox, S.; Pietropaolo, K.; Brown, N. A. *Hepatology* **2005**, *42*, 234A. (d) Brown, N. *Expert. Opin. Invest. Drugs* **2009**, *18*, 709. (e) Huang, Z.; Murray, M. G.; Secrist, J. A., III. *Antiviral Res.* **2006**, *71*, 351. (f) Erhardt, A.; Deterding, K.; Benhamou, Y.; Reiser, M.; Forns, X.; Pol, S.; Calleja, J. L.; Ross, S.; Spangenberg, H. C.; Garcia-Samaniego, J.; Fuchs, M.; Enriquez, J.; Wiegand, J.; Stern, J.; Wu, K.; Kukolj, G.; Marquis, M.; Beaulieu, P.; Nehmiz, G.; Steffgen, J. *Antiviral Therapy* **2009**, *14*, 23–32. (g) Beaulieu, P. L. *Expert Opin. Ther. Pat.* **2009**, *19*, 145–164.

(4) (a) Peng, J. W. *J. Am. Chem. Soc.* **2003**, *125*, 11116–11130. (b) LaPlante, S. R.; Aubry, N.; Deziel, R.; Ni, F.; Xu, P. *J. Am. Chem. Soc.* **2000**, *122*, 12530. (c) Peng, W.; Wilson, B. D.; Namanja, A. T. *J. Biomolecular NMR* **2009**, *45*, 1–2. (d) Peng, J. W. *Structure* **2009**, *17*, 319–320. (e) Mauldin, R. V.; Carroll, M. J.; Lee, A. L. *Structure* **2009**, *17*, 386–394. (f) Taylor, R. E.; Chen, Y.; Beatty, A.; Myles, D. C.; Zhou, Y. *J. Am. Chem. Soc.* **2003**, *125*, 26–27. (g) Thoma, G.; Magnani, J. L.; Patton, J. T.; Ernst, B.; Jahnke, W. *Angew. Chem., Int. Ed.* **2001**, *125*, 1941–1945.

(5) (a) Kramer, B.; Rarey, M.; Lengauer, T. *Proteins* **1999**, *37*, 228. (b) Verdonk, M. L.; Cole, J. C.; Hartshorn, M. J.; Murray, C. W.; Taylor, R. D. *Proteins* **2003**, *52*, 609. (c) Goodsell, D. S. CSH Protoc 2009, 2009 (pdb prot5200); (d) Morris, G. M.; Huey, R.; Olson, A. J. *Curr. Protoc. Bioinformatics* 2008, chapter 8, unit 814; (e) Ewing, T. J.; Makino, S.; Skillman, A. G.; Kuntz, I. D. *J. Comput.-Aided Mol. Des.* **2001**, *15*, 411. (f) McGann, M. R.; Almond, H. R.; Nicholls, A.; Grant, J. A.; Brown, F. K. *Biopolymers* **2003**, *68*, 76. (g) Goto, J.; Kataoka, R.; Muta, H.; Hirayama, N. *J. Chem. Inf. Model.* **2008**, *48*, 583. (h) Tondel, K.; Anderssen, E.; Drablos, F. *J. Comput.-Aided Mol. Des.* **2006**, *20*, 131. (i) Jackson, S.; DeGrado, W.; Dwivedi, A.; Parthasarathy, A.; Higley, A.; Krywko, J.; Rockwell, A.; Markwalder, J.; Wells, G. *J. Am. Chem. Soc.* **1994**, *116*, 3220–3230. (j) Miller, C. P.; Collini, M. D.; Harris, H. A. *Bioorg. Med. Chem. Lett.* **2003**, *13*, 2399–2403. Udugamasooriya, D. G.; Spaller, M. R. *Biopolymers* 2008, *89*, 653–667. (k) Sharma, R.; Lee, J.; Wang, S.; Milne, G. W. A.; Lewin, N. E.; Blumberg, P. M.; Marquez, V. E. *J. Med. Chem.* **1996**, *39*, 19–28. (l) Martin, S. F. *Pure Appl. Chem.* **2007**, *79*, 193–200. (m) Harris, P. W. R.; Hügel, H. M.; Nurlawis, F. *Mol. Simul.* **2002**, *28*, 889–902. (n) Giebel, L. B.; Cass, R.; Milligan, D. L.; Young, D.; Arze, R.; Johnson, C. *Biochemistry* **1995**, *34*, 15430–15435.
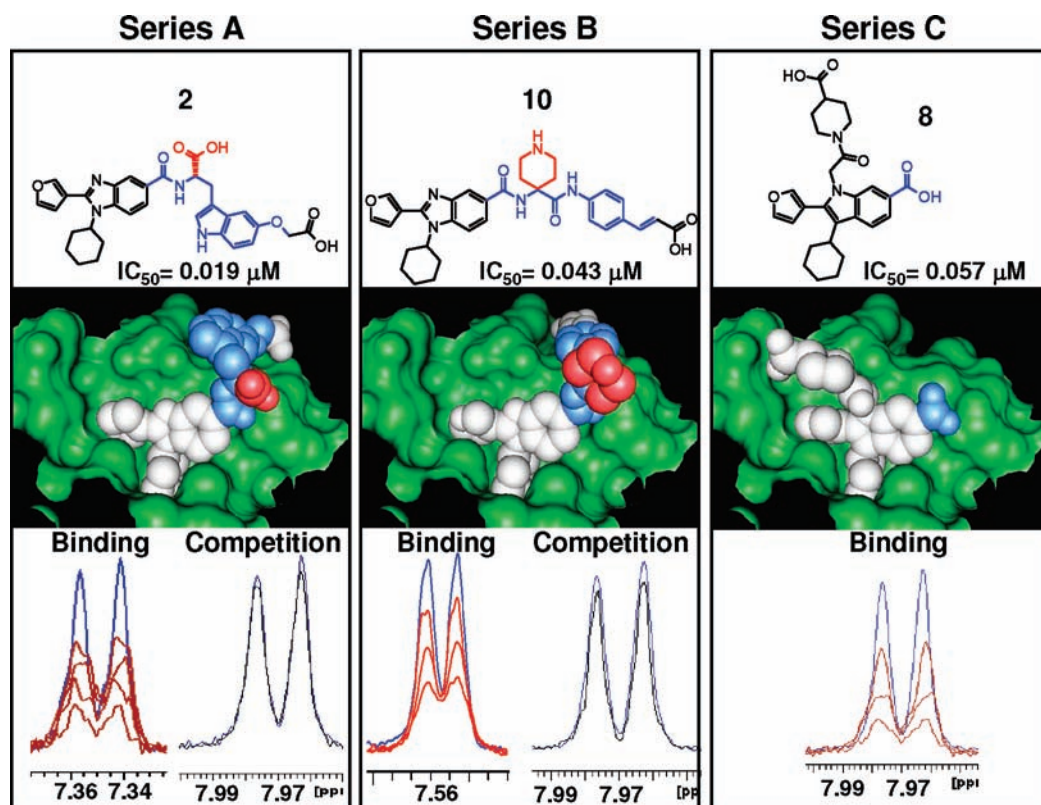
Figure 2. Shown are compounds (colored as white, blue, and red) bound to the allosteric "thumb pocket I" of HCV polymerase (colored green) which were derived from a combination of X-ray, NMR, and docking. (A) The complex involving compound **2** is displayed, and was determined by docking **2** to the pocket using using the X-ray structure shown in Figure 2C as a guide which included overlaying the common benzimidazole cores and cyclohexanes. A representative, low-energy pose is shown which is also consistent with the bound structure reported from tr-NOESY NMR data.[7] Binding of compound **2** to HCV polymerase was confirmed by 600 MHz ^{1}H NMR resonance broadening of **2** upon incremental addition of 0.5 mM stock polymerase. Also, an NMR competition experiment demonstrated that the resonance broadening observed for compound **8** upon addition of polymerase was lost in the presence of compound **2**. (B) The complex involving compound **10** is displayed. It was derived in a similar manner as described in (A) with support from tr-NOESY data (see Supporting Information) and NMR binding and competition experiments. (C) Shown is the X-ray complex[11a] of compound **8** along with NMR binding data.

flexibility in the free and bound states were previously reported in our drug discovery programs aimed at targeting the human cyctomegalovirus protease,[6] the HCV NS3 protease[7a] and NS5B polymerase.[7b] As a result, this knowledge contributed to the design of drug candidates in the later two cases that effectively suppressed HCV viral load in human clinical trials.[3f,8]

Our HCV polymerase drug discovery program is a good illustration of these concepts,[3f,7b,9] and began with a structure and dynamics analysis early during the validation of compound **1** (Figure 1) as an attractive hit from screening a large compound collection. In combination with structure–activity relationships (SAR), we gained a qualitative understanding of the binding roles of the molecular subgroups such as the central benzimidazole scaffold, the structural hinge (blue colored phenethyl-

amide), the critical cyclohexyl, and the more tolerant left-hand side. This evolved into three independent chemical series (Series A–C in Figure 1).

For example, efforts along Series A (Figure 1) revealed that the red-colored carboxylic acid of compound **2** provided potency by rigidifying the free-state conformation to resemble an NMR-derived "L" shape when bound.[7b,9d] The bound model of its complex with HCV polymerase shown here (Figure 2A) and SAR[9d] clearly showed that this acid (red) was exposed to solvent and had no direct interaction with the polymerase. The 48-fold

(6) LaPlante, S. R.; Bonneau, R.; Aubry, N.; Cameron, D. R.; Déziel, R.; Grand-Maître, C.; Plouffe, C.; Tong, L.; Kawai, S. H. *J. Am. Chem. Soc.* **1999**, *121*, 2974–2986.

(7) (a) LaPlante, S. R.; Llinàs-Brunet, M. *Curr. Med. Chem.: Antiinfect. Agents* **2005**, *4*, 111–132. (b) LaPlante, S. R.; Jakalian, A.; Aubry, N.; Bousquet, Y.; Ferland, J. M.; Gillard, J.; Lefebvre, S.; Poirier, M.; Tsantrizos, Y. D.; Kukolj, G.; Beaulieu, P. L. *Angew. Chem., Int. Ed.* **2004**, *43*, 4306–4311.

(8) Lamarre, D.; Anderson, P. C.; Bailey, M.; Beaulieu, P. L.; Bolger, G.; Bonneau, P.; Bös, M.; Cameron, D. R.; Cartier, M.; Cordingley, M. G.; Faucher, A. M.; Goudreau, N.; Kawai, S. H.; Kukolj, G.; Lagacé, L.; LaPlante, S. R.; Narjes, H.; Poupart, M. A.; Rancourt, J.; Sentjens, R. E.; St George, R.; Simoneau, B.; Stelnmann, G.; Thibeault, D.; Tsantrizos, Y. S.; Weldon, S. M.; Yong, C. Y.; Linas-Brunet, M. *Nature* **2003**, *426*, 186.

(9) (a) Beaulieu, P. L.; Bös, M.; Bousquet, Y.; Fazal, G.; Gauthier, J.; Gillard, J.; Goulet, S.; LaPlante, S. L.; Poupart, M. A.; Lefebvre, S.; McKercher, G.; Pellerin, C.; Austel, V.; Kukolj, G. *Bioorg. Med. Chem. Lett.* **2004**, *14*, 119. (b) Beaulieu, P. L.; Bös, M.; Bousquet, Y.; DeRoy, P.; Fazal, G.; Gauthier, J.; Gillard, J.; Goulet, S.; Poupart, M.-A.; Valois, S.; McKercher, G.; Kukolj, G. *Bioorg. Med. Chem. Lett.* **2004**, *14*, 967. (c) Beaulieu, P. L.; Gillard, J.; Bykowski, D.; Brochu, C.; Dansereau, N.; Duceppe, J. S.; Haché, B.; Jakalian, A.; Lagacé, L.; LaPlante, S. R.; McKercher, G.; Moreau, E.; Perreault, S.; Stammers, T.; Thauvette, L.; Warrington, J.; Kukolj, G. *Bioorg. Med. Chem. Lett.* **2006**, *16*, 4987. (d) Beaulieu, P. L.; Bousquet, Y.; Gauthier, J.; Gillard, J.; Marquis, M.; McKercher, G.; Pellerin, C.; Valois, S.; Kukolj, G. *J. Med. Chem.* **2004**, *47*, 6884. (e) Kukolj, G.; McGibbon, G.; McKercher, G.; Marquis, M.; Lefebvre, S.; Thauvette, L.; Gauthier, J.; Goulet, S.; Poupart, M. A.; Beaulieu, P. L. *J. Biol. Chem.* **2005**, *280*, 39260–39267. (f) Goulet, S.; Poupart, M. A.; Gillard, J.; Poirier, M.; Kukolj, G.; Beaulieu, P. L. *Bioorg. Med. Chem. Lett.* **2010**, *20*, 196–200. (g) McKercher, G.; Beaulieu, P. L.; Lamarre, D.; LaPlante, S. R.; LeFebvre, S.; Pellerin, C.; Thauvette, L.; Kukolj, G. *Nucleic Acids Res.* **2004**, *32*, 422.
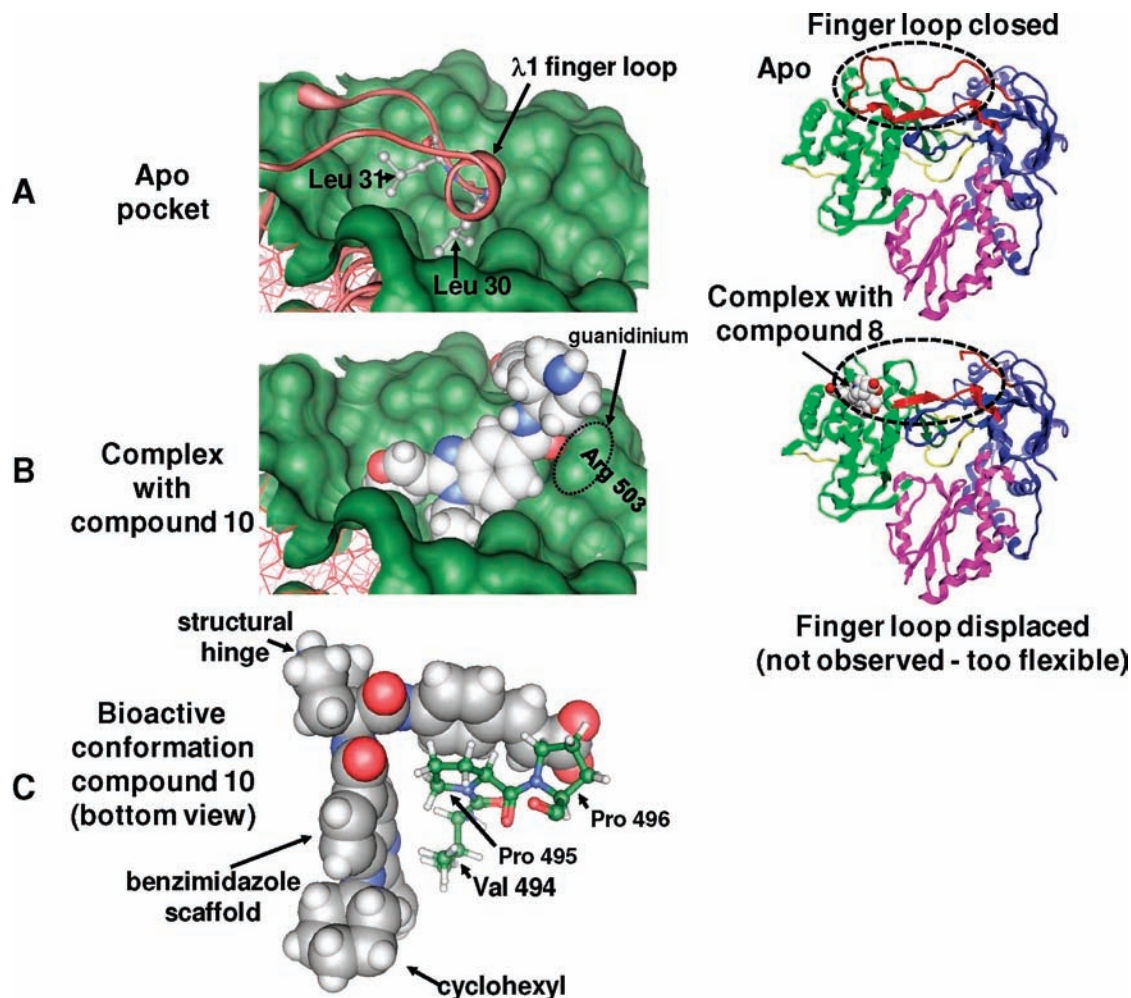
Figure 3. (A) A pocket view and full display of the X-ray structure of apo HCV polymerase is shown.[11a] Encircled is the closed form of the "λ1 finger-loop". The pocket view is rotated 180° along the vertical axis with respect to the full view for visualization purposes. (B) A pocket view of the complex of compound **10** (colored as white, red and blue) with HCV polymerase (colored green) is displayed on the left side, and the full view of the X-ray structure of the complex with compound **8** is shown on the right. Encircled is the unobserved, open form of the "λ1 finger-loop". The pocket view is rotated 180° along the vertical axis with respect to the full view for visualization purposes. (C) A bottom-view of the complex involving **10** is shown to emphasize the importance of multiple weak CH-π interactions involving HCV polymerase Val 494, Pro 495, and Pro 496.

difference in binding affinity gained by addition of this acid demonstrated the benefits of reducing the entropic costs of ligand binding.[7b] Furthermore, knowledge of the acid's role as a "rigidifier" led to its replacement with a heterocyclic isosteres (e.g., thiazole compound **3** in Figure 1). Despite somewhat reduced intrinsic potency, the increase in lipophilicity of compound **3** provided permeability and inhibition of subgenomic HCV RNA replication in a cell-based assay (EC$_{50}$ = 1.7 μM). Although the subsequent replacement of the benzimidazole scaffold with a more lipophilic indole (compound **4**) led to further improvements in cell-culture activity (EC$_{50}$ = 0.05 μM), intractable physicochemical properties compromised any further development as a drug candidate.[9c,f] Given these liabilities, alternate but related series of compounds were pursued.

The truncated compounds of Series C (Figure 1) had attractive features. Similar intrinsic potency could be achieved with multiple changes that exploited alternate interactions with the polymerase pocket. The carboxylic acid in series C forms a better interaction with Arg 503 (*vide infra*, Figure 2C and 3B). Replacement of the benzimidazole with a more lipophilic indole core allows the introduction of an additional appendage on the indole nitrogen that can engage in C—H to carbonyl interactions with Leu 492 and Gly 493 (see Supporting Information). Such

interactions could also account for the potency gain in series A between compounds **3** and **4**.

However, this series suffered from poor cell culture activity and other properties required to advance competitively to the clinic.[10] Regardless, one of the benefits with this series was that X-ray structures were solved for compounds **8**[11a] (as described here) and **9**[11b] bound to HCV polymerase (Figure 2C) which also served as the starting points for creating NMR-supported docking models of the complexes shown in Figure 2A,B (vide infra).

Given that compounds from series A and C had some undesirable properties with regard to advancement as clinical candidates, a third series of compounds was sought and designed; the new series is shown as series B[9f] in Figure 1.

(10) (a) Beaulieu, P. L. *Curr. Opin. Drug Disc.Dev.* **2006**, *9*, 618–626. (b) Harper, S.; Avolio, S.; Pacini, B.; Di Filippo, M.; Altamura, S.; Tomei, L.; Paonessa, G.; Di Marco, S.; Carfì, A.; Giuliano, C.; Padron, J.; Bonelli, F.; Migliaccio, G.; De Francesco, R.; Laufer, R.; Rowley, M.; Narjes, F. *J. Med. Chem.* **2005**, *48*, 4547–4557. (c) Beaulieu, P. L.; Jolicoeur, E.; Gillard, G.; Brochu, C.; Coulombe, R.; Dansereau, N.; Duan, J.; Garneau, M.; Jakalian, A.; Kuhn, P.; Lagace, L.; LaPlante, S. R.; McKercher, G.; Perrault, S.; Poirier, M.; Poupart, M.-A.; Stammers, T.; Thauvette, L.; Thavonekham, B.; Kukolj, G. *Bioorg. Med. Chem. Lett.* **2010**, *20*, 857–861.

Overall, the design was based on the knowledge of the binding mode and role of each substituent from compound **2** of series A.[7b,9f] It was thought that opportunities for new chemical entities could be identified by replacing the blue-colored "structural hinge" and the red-colored acid "rigidifier" of **2**. For this purpose, a rational and novel parallel synthesis strategy[9f] was developed where synthetically feasible replacements were identified that were presumed to access the same spatial and conformational roles. From several small libraries, the diamide cinnamic acid moiety shown in blue in compounds **5** and **6** (Figure 1) was suitable as it allowed us to keep the spatial arrangements of the critical left- and right-side pharmacophores (colored in black on compounds **2,5,6**). The nearly 6-fold potency improvement in IC$_{50}$ observed upon α,α-disubstitution (compound **5** versus **6**, Figure 1) made this new series attractive.

Deriving polymerase complexes with compounds from each series shown in Figure 2 was achieved using a combination of X-ray crystallography, NMR and modeling with support from binding-site resistance mutant studies and photoaffinity labeling experiments. The structure of **8** bound to "thumb pocket I" was determined by X-ray crystallography and is shown in Figure 2C, and when compared to the X-ray structure of apo polymerase, it became clear that **8** required the displacement of the λ1 finger loop from the thumb domain for binding. See the apo and complex views shown in Figure 3.

Attempts to obtain bound crystal structures of compounds from series A and B proved to be difficult due the crstal cracking as described in the Materials and Methods and in the Supporting Information. In short, the crystal quality is likely affected by the dynamic properties of the loop and the conformational changes upon ligand binding. Therefore, binding site determinations had to be secured by NMR binding and competition experiments. As a control, it was first demonstrated that compound **8** experienced NMR line-broadening (DLB) upon incremental addition of HCV polymerase (red), as a result of reversible fast-exchange binding. The data are displayed at the bottom of Series C in Figure 2, where the resonance of free **8** (blue) broadened (red) upon incremental addition of small aounts of stock 0.5 mM HCV polymerase. This showed that compound **8** binds to HCV polymerase, as also demonstrated by the X-ray structure shown in Figure 2 Series C. Likewise, NMR binding studies confirmed that compounds **2** and **10** also bind to HCV polymerase (DLB data shown at the bottom of Series A and B in Figure 2). Subsequent NMR competition experiments on samples containing compound **8** (as a probe or spy molecule) with HCV polymerase showed that its resonance (colored black at the bottom of Series A and B) no longer broadens upon addition of **2** and **10**. In fact, it resembles that of the blue resonance of **8** of the free state, suggesting that it is prevented from binding to the pocket.

Overall, the ensemble of data is consistent with compounds **2** and **10** binding at the same "thumb pocket 1" site as **8**. Our confidence that these compounds bind to the same site was also corroborated by resistant mutant and photoaffinity labeling studies. We were able to locate the binding region using a photoaffinity label on an analogue of compound **2** from series A, and resistant mutants were selected at Pro 495 and Pro 496 in the presence of compound **6** of Series B.[9e] A close-up view at Figure 3C shows that these amino acids are located at "thumb pocket 1" and lie in close proximity to the critical L-shape created by compounds **2** and **6** in the complex. In summary, the ensemble of data acquired here and described elsewhere (including appropriate inhibition curves, counterscreen assays,

^{19}F NMR, kinetics and mechanistic studies, etc) are consistent with specific binding to the HCV polymerase.[7b,9,10]

The bioactive conformation of compounds **2**[7b] and **10** were then determined by NMR transferred NOESY (tr-NOESY) experiments[12] (see also Supporting Information) when bound to HCV polymerase. Modeling calculations then helped to dock these compounds into "thumb pocket I" in a fashion similar to that found in the X-ray structure of compound **8**[11a] (Figure 2C); which included overlaying the common benzimidazole cores and cyclohexanes. Again, this was also corroborated by binding-site resistance mutant studies which suggested that inhibitors bound close to Pro 495 and Pro 496.[9e] The transferred NOESY distance information extracted from the bound-states were also consistent with the bioactive "L" shape of compounds **2** and **10** in Figure 2A,B.

The NMR-consistent models involving compounds **2** and **10** revealed notable features. For example, the role of the blue-colored structural hinge became apparent as its curved shape positioned the right-side aromatic rings over the ledge formed by Val 494 and Pro 495 onto a plateau formed by Pro 495 and Pro 496 (Figure 3C), which were earlier identified as part of the binding site by a resistant mutant study.[9e] The bioactive "L" conformation of compound **10** is clearly stabilized by a significant network of weak interactions involving C—H's from Val 494, Pro 495, and Pro 496 to the aromatic rings of the benzimidazole scaffold and the right-side moiety as shown in Figure 3C. The guanidinium of Arg 503 further stabilizes this complex by hydrogen bonding with the left-side amide carbonyl of **10** as shown in Figure 3B.

The complex involving compound **10** in Figure 2 also revealed that the red-colored piperidine is completely solvent exposed and does not form any direct interactions with the polymerase pocket. When compared to the glycine analogue **5**, addition of the piperidine group resulted in a 6.5-fold improvement in intrinsic potency. Given that this group is solvent-exposed in the bound-state, it may contribute to potency by promoting the bioactive conformation in the free-state; this could also explain the potency improvements for the other α,α-disubstituted analogues **6**, **10**, **13**, and **15** relative to the glycine analogue **5**.

Molecular dynamics calculations are a practical means of exploring the free-state, conformational properties of ligands,[13] and our simulations also supported the above interpretation. It was evident in the data in Figure 4 that the naked glycine analogue **5** sampled a wider range of S1 and S2 torsional angles over time (solid bars in Figure 4B,C), indicative of it sampling a variety of conformations, whereas only a narrow range of the more favorable, bound-like conformations was sampled for **6** and localized around 80° and 70° for S1 and S2 in Figure 4B,C, respectively. Clearly, the more active cyclobutyl analogue **6** prefers to adapt a narrower range of conformations in the free-state (diamond lines and points in Figure 4) that are a better match to the bound-state. In a sense, the cyclobutyl helps to

(11) (a) PDB accession codes 3MWV for the apo HCV polymerase, and 3MWW for the complex with inhibitor **8**. (b) PDB code 2BRK: Di Marco, S.; Volpari, C.; Tomei, L.; Altamura, S.; Harper, S.; Narjes, F.; Koch, U.; Rowley, M.; De Francesco, R.; Migliaccio, G.; Carfí, A. *J. Biol. Chem.* **2005**, *280*, 29765–29770.
(12) (a) Ni, F. *Prog. NMR Spect.* **1994**, *26*, 517. (b) LaPlante, S. R.; Aubry, N.; Bonneau, P.; Kukolj, G.; Lamarre, D.; Lefebvre, S.; Li, H.; Llinàs-Brunet, M.; Plouffe, C.; Cameron, D. R. *Bioorg. Med. Chem. Lett.* **2000**, *10*, 2271.
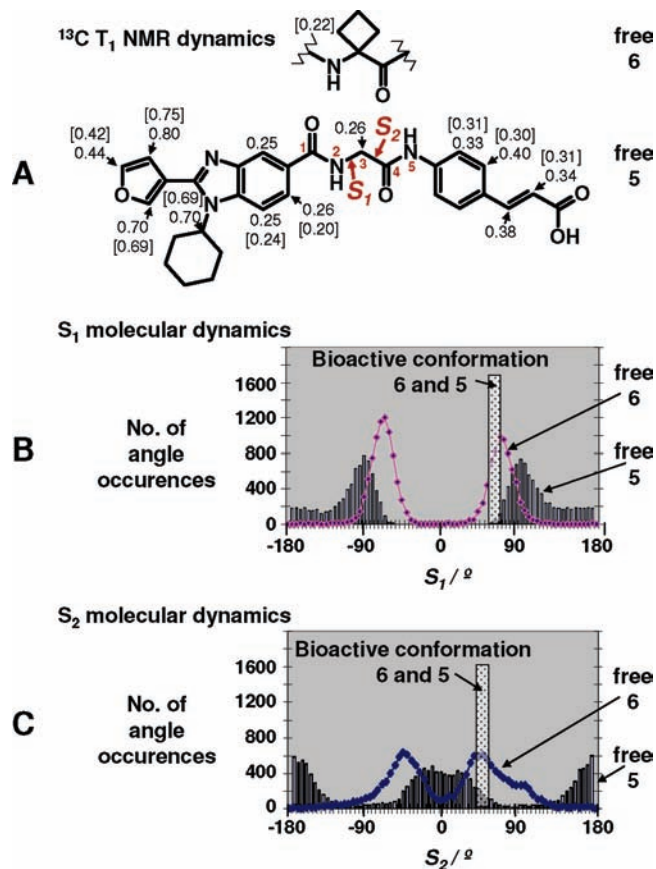(13) Hao, M.-H.; Muegge, I. *J. Chem. Inf. Model.* **2007**, *47*, 2242–2252.

Figure 4. (A) Compounds **5** and **6** are shown along with free-state ^{13}C NMR (125 MHz) NT_1 relaxation times (seconds). The NT_1 data are displayed beside each carbon atom for compound **5**, and data for compound **6** are given within square brackets. The samples were prepared in DMSO-d$_6$ solvent and data were acquired as described elsewhere.[4b,7b] In cases where two hydrogens are attached to a single carbon, NT_1 data are given (the product of the number of attached protons and the longitudinal relaxation time). Note that due to the symmetry of the phenyl, only two relaxation data points are observed and reported. (B) Molecular dynamics histograms are shown for the number of angular occurrences for each torsion angles of S1 for compounds **5** and **6** in the free-state. See Figure 4A for a definition of the S1 torsion angle. (C) Molecular dynamics histograms are shown for the number of angular occurrences for each torsion angles of S2 for compounds **5** and **6** in the free-state. See Figure 4A for the definition of the S2 torsion angle.
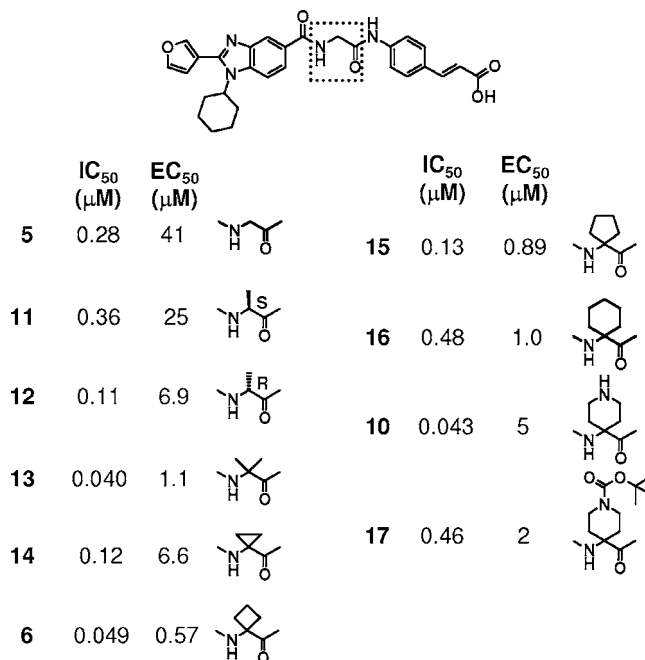

Figure 5. Analogues of series B are shown. See the Supporting Information for synthetic schemes and characterization. Methods for determining activities against HCV NS5B polymerase (genotype 1b) are also described in the Supporting Information and elsewhere.[9g] The activity values are the mean from multiple determinations with the following IC$_{50}$ and EC$_{50}$ standard deviations, respectively: **5**, ± 0.07, ± 20[a]; **11**, ± 0.08, ± 8; **12**, ± 0.06, ± 1.6; **13**, ± 0.04, ± 0.4; **14**, ± 0.03, ± 0.8; **6**, ± 0.05, ± 0.2; **15**, ± 0.03, ± 0.12; **16**, ± 0.013, ± 0.04; **10**, ± 0.01, ± 2.5[a]; **17**, ± 0.23[a], ± 1[a]. [a]Standard deviations were overestimated at 50% of the activity values but are typically much less.

"fine-tune" the structural hinge to resemble the bioactive conformation.

^{13}C spin−lattice relaxation (^{13}C T$_1$) experiments were employed as an NMR parameter for monitoring the relative flexibility of C−H vectors. As a method which is sensitive to motions on the pico- to nanosecond time scales, shorter relaxation times are typically indicative of relatively slower segmental motion or flexibility. The T_1 times reported here result from the collection of a single set of experiments, and an error range of ±12% is anticipated (see Supporting Information). Overall, much longer T_1 times were not observed for either the glycine **5** or the cyclobutyl **6** analogues, as observed with flexible compounds in other programs,[6,7] suggesting that the diamide hinge effectively reduces the flexibility of the inhibitors. It may be noteworthy in Figure 4A that the glycine analogue **5** has slightly longer T_1 times in general (but close to the anticipated error range) as compared to the cylcobutyl compound **6**, which could be reflective of an limited increase in flexibility that also goes beyond the local torsion angles S1 and S2.

Conformational selection and an inhibitor's flexibility in the free-state likely influence many drug discovery programs. It may account for the frequently observed phenomenon of nonlinear SAR trends, which can be analyzed using "box analyses".[14] For example, one would not have expected the 7-fold improvement in potency of the gem-dimethyl analogue **13** relative to the naked glycine **5** (Figure 5), considering that the (R) alanine analogue (compounds **12**) resulted in only a 2.5-fold improvement over **5**, whereas the (S)-distomer had comparable activity to **5**.[9f] The potencies of the two alanine analogues simply are not additive based on the improvement observed for the gem-dimethyl analogue, and highlights the importance of conformational selection and entropy in drug discovery.

The important role of the diamide segment described herein can also help to decipher the SAR impact of multiple substituents shown in Figure 5. For example, the cyclopropyl moiety in compound **14** shown in Figure 5 resulted in a 3-fold loss in potency compared to the closely related dimethyl **13** because the cyclopropyl imparted an unfavorable angle involving the αC center.[15] The larger ring sizes of compounds **15** and **16** perturb the free-state population away from the bioactive

(14) (a) Kawai, S. H.; Bailey, M. D.; Halmos, T.; Forgione, P.; LaPlante, S. R.; Llinàs-Brunet, M.; Naud, J.; Goudreau, N. *ChemMedChem* **2008**, *3*, 1654–1657. (b) Cockroft, S. L.; Hunter, C. A. *Chem. Soc. Rev.* **2006**, *36*, 172–188. (c) Adams, H.; Carver, F. J.; Hunter, C. A.; Morales, J. C.; Seward, E. M. *Angew. Chem., Int. Ed.* **1996**, *35*, 1542–1544. (d) Fischer, F. R.; Schweizer, W. B.; Diederich, F. *Angew. Chem., Int. Ed.* **2007**, *46*, 8270–8273.

(15) (a) Pirrung, M. C. *J. Org. Chem.* **1987**, *52*, 4179. (b) Valle, G.; Crisma, M.; Toniolo, C.; Holt, E. M.; Tamura, M.; Bland, J. *Int. J. Pept. Protein Res.* **1989**, *34*, 56. (c) Di Blasio, B.; Pavone, V.; Pedone, C. *Cryst. Struct. Commun.* **1977**, *6*, 745.

conformation by the introduction of various chair/boat puckering that affect the S1 and S2 torsion angles (defined in Figure 4). This is more evident when one compares the 10-fold activity difference between **16** and **10**, which also differ significantly in S1 and S2 energy torsion profiles and free-state conformations as determined by NMR. The incorporation of a nitrogen as shown in **10** favors the bioactive free-state population along torsion angles S1 and S2 as compared to the carbocycle **16** (see Supporting Information). Finally, the subsequent addition of a large BOC group as in compound **17** again alters the free-state chair/boat and S1/S2 free-state equilibrium, resulting in a 10-fold loss in potency compared to **10**. The reasonable activity of compound **17** is nonetheless informative in that the addition of the bulky BOC group on the nitrogen is consistent with the hinge being exposed to solvent in the complex.

The polymerase "thumb pocket I" undergoes major changes upon ligand binding. An X-ray structure of apo HCV polymerase is displayed in Figure 3A, which reveals that the "$\lambda 1$ finger-loop" naturally occupies this polymerase pocket as deduced from well-defined electron density. However, compound **8** occupies this pocket in the complex, as shown in Figure 3B, and there is a lack of electron density for the loop residues. Overall, this suggests that the loop adopts a disengaged conformation (i.e., loop residues are displaced, exposed to solvent, and flexible). The precise mechanism that results in the release of the $\lambda 1$-loop from the pocket is unclear, however, the disengaged state likely exists at a low-level population in the apo form and reversible ligand binding shifts the equilibrium toward this alternate complex state. The displacement and increased flexibility of the finger loop was also consistent with ^{15}N TROSY NMR experiments, where a new subset of sharper crosspeaks appeared upon the addition of compound **8** as compared to the ^{15}N TROSY spectra of apo polymerase (see Supporting Information).

Notably, we recently reported[9e] that the L30R and L30S mutant constructs at the tip of the $\lambda 1$ finger-loop resulted in a ~100-fold improvement in affinity for compound **8**, suggesting that the mutant constructs further shift the equilibrium to the disengaged state relative to wild-type. These results are also consistent with a receptor conformation selection mechanism for inhibitor binding, and the $\lambda 1$ loop conformational changes are critical for compound binding and pharmacological inhibition of HCV polymerase function.

Materials and Methods

HCV NS5B Polymerase Constructs for IC$_{50}$ Activity Assays and NMR/X-ray Crystallography. HCV genotype 1b NS5B strain 1b-40 and J4 were used to clone into baculovirus and *E. coli* expression vectors.[9g] The full length HCV NS5B polymerase used for compound IC$_{50}$ determination was expressed as a hexa-histidine fusion protein in baculovirus infected cells and purified by metal chelating chromatography on Ni^{2+} column followed by DEAE-sepharose and heparin-sepharose chromatography. The preparation was homogeneous by SDS-PAGE analysis and used at 10 nM in the standard HCV polymerase assay. This scintillation proximity assay uses 0.5 μCi of [^{3}H]-UTP, 1 μM UTP, 250 nM 5'-biotinylated oligo(rU$_{12}$), 10 μg/mL poly(rA) in 20 mM Tris-HCl pH 7.5, 5 mM MgCl$_2$, 1 mM EDTA, 1 mM DTT, 0.2 U/μL of RNasin, 5% DMSO, 3% glycerol, 30 mM NaCl, 0.33% dodecyl-β-D-maltoside, 0.01% IGEPAL. The 60-μL reaction was terminated after 90 min at 22 °C by the addition of 20 μL of stop solution (150 μg/mL of tRNA in 0.5 M EDTA) and 30 μL of streptavidin-coated beads (8 mg/mL in 20 mM Tris-HCl pH 7.5, 25 mM KCl, 0.025% (w/v) sodium azide) for Scintillation Proximity Assay (Perkin-Elmer). After 30 min at room temperature, 75 μL of 5 M cesium chloride were added

to the wells and the plate was left at room temperature for one hour before quantifying the radioactive UMP incorporated onto the biotinylated primer by counting for 60 s on a TopCount (Packard). From serial dilution of the test compound, the percent inhibition was plotted against the compound concentration and a nonlinear curve was fitted (Hill model) to the % inhibition-concentration data. The calculated % inhibition values were then used to determine the median inhibitory concentration IC$_{50}$, slope factor (n) and maximum inhibition (I_{max}) by the nonlinear regression procedure of SAS (Statistical Software System, SAS Institute Inc., Cary, N.C.)

Protein for NMR experiments were prepared from constructs expressing soluble versions that lack the C-terminal 21 amino acids and encode a C-terminal hexa-histidine tag,[9g] purified as described above, exchanged with deuterated buffer components (20 mM Tris d-$_{11}$ pH 7.5, 10% glycerol d-$_8$, 2 mM DTT d-$_{10}$, 1 mM EDTA D-$_{16}$, 300 mM NaCl) and concentrated. The genotype 1b J4 strain NS5B lacking the C-terminal 21 amino acids and encoding a C-terminal hexa-histidine tag (HCVNS5B1bJ4-ΔC21$-$H6) was used for X-ray crystallography and also expressed in *E. coli* in ^{15}N labeled bacterial growth medium and purified for use in TROSY experiments. The HCVNS5B1bJ4-ΔC21$-$H6 used for X-ray crystallography was purified as described above, further concentrated on Hi-Trap SP column and then subjected to size exclusion chromatography on a Superdex-200 column to obtain a homogeneous, monomeric and highly purified preparation.

Determination of X-ray Structures of Apo HCV Polymerase and Inhibitor Complex. Crystallization of apo protein proceeded as follows. Crystal of HCVNS5B1bJ4-ΔC21$-$H6 were grown by the hanging drop technique using Nextal's plates (Qiagen). The well solution consisted of 100 mM MES pH 5.4, 21% PEG5000 mme, 400 mM ammonium sulfate and 10% glycerol. The crystallization drops were made of 1 μL of the well solution and 1 μL of protein solution at a concentration of 7.7 mg/mL in the final purification buffer (20 mM tris pH 7.5, 300 mM NaCl, 10% glycerol and 5 mM DTT). The crystallization plate was then incubated at 11 degree. Large crystals were observed within a week.

Inhibitor soaking proceeded as follows. The NS5B crystals were very sensitive to solution transfer. Eventually, crystals were successfully transferred in a 5 μL drop of a soaking solution copying the content of crystallization drop at the end of the vapor diffusion experiment. The pH of the buffer was raised to be more similar to assay conditions. The soaking solution was made of 14% PEG5Kmme, 14 mM tris pH 7.5, 70 mM TES pH 7.0, 14%glycerol, 210 mM NaCl, 10 mg/mL lysozyme, and 280 mM ammonium sulfate. The inhibitor molecule was dissolved in DMSO to a concentration of 25 mM and 0.2 μL of this inhibitor stock solution was added to the 5 μL soaking drop. The crystallization support was screwed back on top of the well solution and let untouched for 5 h at 11 °C. After incubation, the crystal was transfer in a cryoloop (Hampton Research, California, USA), plunged and stored in liquid nitrogen prior diffraction data collection.

It was found that upon inhibitor soaking the lattice of the crystal was affected such as the resolution of the diffraction pattern is diminished proportionally to soaking time. Although an apo crystal could be soaked in the described soaking solution for more than 24 h and still diffract to 2.2 Å resolution, a same soaking time in presence of an inhibitor molecule resulted in a reduced resolution limit to worst than 3 Å. Optimal e-density maps were obtained with a soaking time of 5 h. This time was enough to obtain sufficient occupancy of the inhibitor molecule while keeping the diffraction to a resolution that allow clear interpretation.

For the structure determinations and refinements, the diffraction data of the apo NS5B were phased by Molecular Replacement (MR) using publicly available structure of HCV NS5B (pdb code: 1C2P). Rotation and translation search were done using the program CNX (Accelrys). Model building was carried out with the software O

(Alwyn Jones, Upsala University, Sweden),[16] and model refinement was performed with the CNX software (Accelrys). The new model was improved by a cycling procedure of model rebuilding and refinement steps. The final model include two molecules of NS5B (residues A1-A149, A154 to A563, B1 to B147, and B153 to B563). The tip of the Λ2 finger loop (150−152) appeared to be flexible and was not modeled. See the Table S1 in the Supporting Information for the refinement statistics.

The structure of the complex involving compound **8** was solved by MR using the apo structure as a model. On the second cycle, the residues B18 to B35 were removed as the initial density map was indicating a clear conformation change of that loop. The subsequent difference e-density maps revealed a clear density for the inhibitor molecule on the newly exposed surface of the thumb domain. The final model includes two molecules of NS5B (residue A1 to A149, A154 to A563, B1 to B17, B36 to B148, and B153 to B563) and one molecule of compound **8** associated with NS5B chain B. See Table S1 in the Supporting Information for refinement statistics.

Despite the medium resolution of the data, most of the inhibitor molecule was well-defined in the e-density maps with the exception of the (*N*-acetyl substitution) which should be considered as flexible. Also, the exact orientation of the furan group is not clearly defined by the data as no H-bond interaction was found to differentiate the oxygen atoms from the carbon of the ring.

X-ray data collection and refinement statistics are provided in the Supporting Information. Also, both structures have been deposited in the Protein Data Bank (accession code 3MWV and 3MWW for the apo and the inhibitor complex respectively).

NMR Binding and Competition Experiments. NMR experiments were performed on Bruker Avance spectrometers (400 and/or 600 MHz ^{1}H frequency) at 27 °C, unless otherwise stated.

Samples to be used for NMR binding and competition experiments were prepared by adding concentrated inhibitor in DMSO-d_6 (typically 0.3 mgs. of compound) to an aqueous buffer composed of 20 mM Tris-d_{11}, 2 mM DTT-d_{10}, 1 mM EDTA-d_{12}, 300 mM NaCl, and 10% (v/v) D_2O spiked with TSP-2,2,3,3-d_4. Buffer was added to a final volume of 600 μL, and the pH was adjusted to 6.0 with diluted HCl. Spectra of free compound at 0.2 mM were then acquired. A concentrated stock solution of HCV polymerase was then added at less than stochiometric amounts to the NMR tube, and spectra were again acquired at each increment such that the inhibitor to polymerase ratio ranged from 40:1 to 10:1. The polymerase stock solution contained 0.5 mM HCV polymerase (NS5BΔ21C−His$_6$) in buffer consisting of 20 mM Tris-d_{11}, 2 mM DTT-d_{10}, 1 mM EDTA-d_{12}, 300 mM NaCl, and 10% (v/v) glycerol-d_8. NOESY spectra were also collected on these samples. For competition experiments, concentrated stock solutions of other compounds were added to the NMR tube followed by the acquisition of spectra. TROSY NMR experiments were run using 26 μM NS5BΔ21C-His$_6$ (1b/J4) labeled with 15N in Tris-d11 25 mM, pH 7.5, NaCl 150 mM, glycerol-d8 5%, TCEP-d16 1 mM.

For spectra acquired on samples in buffer, suppression of the solvent signal was achieved by the use of presaturation or by inserting a 3−9−19 WATERGATE module prior to data acquisition. NOESY experiments on sample tubes containing no polymerase resulted in the observation of no significant cross-peaks. However, NOESY spectra on sample tubes containing polymerase resulted in the observation of many cross-peaks which contained the valuable interhydrogen distance information of the compound when bound to HCV polymerase. Thus, a series of NOESY spectra were typically acquired on these latter samples which included the following mixing times 50, 100, 200, and 300 ms (600 MHz). NOESY crosspeak volumes were scaled and converted to apparent interproton distances. The derived distances were normalized via comparisons with the volumes from an internal fixed interhydrogen distance.

All data sets were processed using the TOPSPIN or WinNMR software (Bruker Canada, Milton, Ontario) and software. Data sets were typically zero-filled to yield 2048 (f2) × 1024 (f1) points after Fourier transformation using a shifted sine-bell window function. [1]H and ^{13}C spectra were chemical shift calibrated relative to the standard values attributed to the DMSO peaks (2.49 and 39.51 ppm, respectively).

Molecular Dynamics Simulations and Docking. Molecular dynamics (MD) simulations were performed for compounds **5** and **6** to generate free-state conformational histograms for angles S1 and S2 as shown in Figure 4. Each compound was first submitted to a conformation sampling to generate 10 diverse conformations that were then, each, submitted to 1 ns. MD run. The MD simulations were run with MOE (versions 2008.10) under constant volume and constant temperature conditions using MMFF94 (as implemented in MOE version 2008.10). Each MD simulation consisted of a heating phase that gradually increased the system temperature from 0 K to 298 K in 10 ps, followed by a equilibration phase at the target temperature of 298 K for 10 ps. The production phase (data accumulation phase) consisted of 1 ns and snapshots of the system were recorded every 0.5 ps. The nonbonded cutoff radius was set to infinity and an implicit solvation model was used to mimic an aqueous environment. The production phase trajectories of the 10 MD runs were then combined to analyze the S1 and S2 angles with the Conformation Geometries module of MOE.

Compounds were docked to the allosteric "thumb pocket I" of HCV polymerase using Glide (version 2007) in XP mode and with the use of experimentally derived structures from X-ray crystallography and bound-state information from NMR binding and competition studies.

Conclusions

In the context of deriving novel inhibitors of HCV polymerase, the bimolecular recognition we described here may be represented by the collision of two flexible objects. Recognition involves a disengaged "finger loop" from an allosteric site of the thumb domain of the polymerase, and binding of ligands in the bioactive "L" conformation (series A and B). From a ligand design perspective, the work described here presents a good example of how a ligand's "structural hinge" influences potency, and due to its solvent exposure in the complex, reasonable structure−activity-relationships can be interpreted. Although the other segments of the inhibitors in series A, B, and C are also important for potency, such as the cyclohexyl and the lipophilic benzimidazole/indole cores, the structural hinge can impart significant potency that can be "fine tuned". Moreover, variants of the hinge also significantly influence cell culture activity and other properties, which ultimately allowed us to successfully transition from compounds that had poor physicochemical and pharmacodynamic properties (series A) to a more promising series (series B). As expected, the improvements in cell culture potency observed in series A upon replacement of the benzimidazole by an indole core (compounds **3** to **4**) were also translated in the new series B (compounds **6** to **7**), and likely arise from an increase in lipophilic character (and cell membrane permeability).

Overall, compound **7** maintains good enzymatic potency and has an impressive cell-culture potency (IC$_{50}$ = 0.095 μM, EC$_{50}$ = 0.072 μM,). Unlike compound **4**, it also has beneficial physicochemical and pharmacokinetic properties that promise new opportunities for progress toward the development of novel HCV therapeutics in the clinic. Indeed, a close analogue of compound **7** has shown antiviral effects in clinic studies.[3f]

(16) Jones, T. A.; Zou, J.-Y.; Cowan, S. W.; Kjeldgaarrd, M. *Acta Crystallogr.* **1991**, *A47*, 110–119.

Supporting Information Available: Additional materials and methods information are provided that include: X-ray data collection and refinement statistics for the apo and inhibitor complex, NMR materials and methods, more information on competition and binding site determinations, a comformational comparison of compounds **10** and **16** in the free state, NMR data on compound **10** binding to HCV polymerase in solution, and details regarding inhibitor synthesis and characterization. This material is available free of charge via the Internet at http://pubs.acs.org.

JA101358S